Tetrahedron 64 (2008) 5392–5403

Contents lists available at ScienceDirect

Tetrahedron

journal homepage: www.elsevier.com/locate/tet

Binding studies of a protonated dioxatetraazamacrocycle with carboxylate substrates

Sílvia Carvalho [a], Rita Delgado [a,b,*], Michael G.B. Drew [c], Vânia Calisto [d], Vítor Félix [d]

[a] Instituto de Tecnologia Química e Biológica, UNL, Apartado 127, 2781-901 Oeiras, Portugal
[b] Instituto Superior Técnico, Av. Rovisco Pais, 1049-001 Lisboa, Portugal
[c] School of Chemistry, University of Reading, Whiteknights, Reading RG6 6AD, UK
[d] Departamento de Química, CICECO, Universidade de Aveiro, 3810-193 Aveiro, Portugal

ARTICLE INFO

Article history:
Received 25 January 2008
Received in revised form 26 February 2008
Accepted 3 March 2008
Available online 7 March 2008

Keywords:
Recognition of anions
Dioxatetraazamacrocycle
Binding constants
Molecular dynamics simulations
^{1}H NMR
Potentiometry

ABSTRACT

The tetraprotonated form of the dioxatetraazamacrocycle, 6,19-dioxa-3,9,16,22-tetraaza[22.2.2.2^{11,14}]-triaconta-1(26),11,13,24,27,29-hexaene, $(H_4L^1)^{4+}$, was used as the receptor for binding studies with carboxylate anionic substrates of different shapes, sizes, and charges [succinate (suc^{2-}), cyclohexanetricarboxylate (cta^{3-}), phthalate (ph^{2-}), isophthalate (iph^{2-}), terephthalate (tph^{2-}), and benezenetricarboxylate (btc^{3-})]. Association constants were determined by potentiometry in aqueous solution at 298.2 K and 0.10 M KCl and by ^{1}H NMR titration in D_2O. The strongest association was found for the btc^{3-} anion at 5–7 pH region. From both techniques it was possible to establish the binding preference trend of the receptor for the different substrates, and the ^{1}H NMR spectroscopy gave important suggestions about the type of interactions between partners and the location of the substrates in the supramolecular entities formed. The effective binding constants at pH 6 follow the order: $btc^{3-}>iph^{2-}>cta^{3-}\approx ph^{2-}>tph^{2-}>suc^{2-}$. All the studies suggest that the anionic substrates bind to the receptor via N–H···O=C hydrogen bonds and electrostatic interactions, and the aromatic substrates can also establish π–π stacking interactions. The crystal structures of $(H_4L^1)^{4+}$ and its supramolecular assemblies with ph^{2-} and tph^{2-} were determined by X-ray diffraction. The last two structures showed that the association process in solid state occurs via multiple N–H···O=C hydrogen bonds with the anionic substrate located outside the macrocyclic cavity of the receptor. Molecular dynamics simulations carried out for the association of $(H_4L^1)^{4+}$ with tph^{2-} and btc^{3-} in water solution established at atomic level the existence of all interactions suggested by the experimental studies, which act cooperatively in the binding process. Furthermore, the binding free energies were estimated and the values are in agreement with the experimental ones, indicating that the binding of these two anionic substrates occurs into the receptor cavity. However, the tph^{2-} has also propensity to leave the macrocyclic cavity and its molecular recognition can also happen at the top of the receptor.

1. Introduction

Recognition of anionic substrates has contributed strongly to the development of the supramolecular chemistry in the last decades.[1–8] Due to their important role in biological, industrial, and environmental fields, these substrates are one of the most studied species. Carboxylate anions, for example, are used in diverse industries such as plastic, pharmaceutical, and food. In addition, carboxylate groups are also present in many pesticides and are the active groups in many biological processes. Water is generally used, which is the solvent where these recognition processes are more difficult.[1,9]

The recognition process of carboxylate anions in water is governed by multiple factors, acting in a cooperative fashion, not all completely understood. Different kinds of receptors have been used,[10–13] among them are protonated polyazamacrocyles.[14–28] These receptors offer the possibility of recognition of carboxylates via strong ion–ion electrostatic interactions assisted by multiple hydrogen bonding formation. In spite of this, even in cases where the shape and size between the partners seem to match well, the corresponding association constants are low. Effects such as the type of the receptor counterion or possible repulsions between parts of the partners seem to play an important role.

Trying to contribute to the clarification of the recognition process of anions, in the present work the tetraprotonated

* Corresponding author at present address: Instituto de Tecnologia Química e Biológica, UNL, Apartado 127, 2781-901 Oeiras, Portugal. Tel.: +351 214 46 97 37/8; fax: +351 214 41 12 77.
E-mail address: delgado@itqb.unl.pt (R. Delgado).

0040-4020/$ – see front matter © 2008 Elsevier Ltd. All rights reserved.
doi:10.1016/j.tet.2008.03.002

dioxatetraazamacrocycle (L^1) (Scheme 1) was used as the receptor for di- and tri-, aromatic and aliphatic, carboxylates anions (suc^{2-}, cta^{3-}, ph^{2-}, iph^{2-}, tph^{2-}, and btc^{3-}, see also Scheme 1) in aqueous solution. The X-ray structure of $(H_4L^1)(PF_6)_4$ showed that this macrocycle forms a rectangular cavity, which should be appropriate to recognize planar organic anions by a combination of hydrogen bonds, π–π stacking, and electrostatic interactions. Potentiometric and ^1H NMR spectroscopic studies were carried out to evaluate the binding ability of the receptor for the selected anionic substrates. The crystal structures of $[(H_4L^1)_2(tph)](PF_6)_2$ and $[(H_4L^1)_2(ph)](PF_6)_2$ were determined and showed that the anions are encapsulated between two macrocyclic molecules. For a further insight into the nature of binding between the receptor and two aromatic dicarboxylate anions (tph^{2-} and btc^{3-}), molecular dynamics simulations in periodic boxes of water solvent molecules were also carried out.

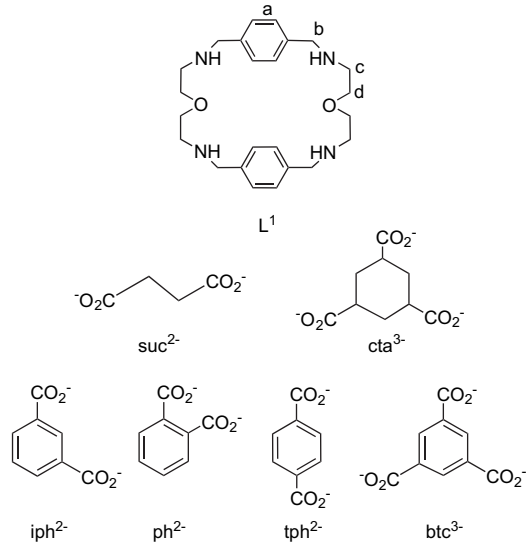

Scheme 1.

2. Results and discussion

2.1. Solution binding measurements

2.1.1. Potentiometric studies

The association constants of the receptor $(H_iL^1)^{i+}$ with several carboxylate anions, suc^{2-}, cta^{3-}, ph^{2-}, iph^{2-}, tph^{2-} and btc^{3-}, were determined in aqueous solutions at 298.2 K and 0.10 M KCl using the HYPERQUAD program.[29] The values obtained are collected in Table 1. The protonation constants of $(H_4L^1)^{4+}$ were determined in the same experimental conditions, and the values of the stepwise constants are: $\log K_1^H=9.42(1)$; $\log K_2^H=8.74(1)$; $\log K_3^H=7.86(1)$; $\log K_4^H=7.05(1)$ [$\log \beta_4^H=33.07(1)$]. The small differences observed from the previously reported in 0.10 M KNO_3[30] should be ascribed to the different salts used to maintain the ionic strength. The protonation constants of the anionic substrates contribute significantly to the final association constants; therefore, the values were also determined in our experimental conditions.[24,28]

At pH≈6, the receptor is predominantly in its higher charged form [$(H_4L^1)^{4+}$ >95%, Fig. 1], favoring the electrostatic interactions with anionic substrates, and on the other hand it is the pH at which most of the studied anions are completely deprotonated. All the spectroscopic measurements were then performed at this pH. However, several assembled species with different number of protons are formed in the entire pH range. Potentiometry is the most accurate technique for the quantitative evaluation of equilibrium constants of systems with such complexity.

These data show that only species of 1:1 receptor to substrate stoichiometry were found for all the studied cases, although several species with different protonation states were determined. However, the comparison of overall constants of the same receptor and substrates having different basicities, or different receptors and the same substrate, or even to establish the correct stepwise equilibria at each pH, it is not straightforward task. The calculation of the effective association constant is the easiest way to take into account the different competition between each anion and the proton for the receptor,[23,31] which is defined as $K_{eff}=\Sigma[H_{i+j}AL]/(\Sigma[H_iA]\times\Sigma[H_jL])$. In Figure 2, the plot of the effective constants for the studied anions is shown.

It can be stated, based on the diagram of Figure 2, that at pH≈6 the associated species $H_4L^1A^{2+/+}$ (the charge of this entity depends on the charge of the anion) is formed by the reaction $(H_4L^1)^{4+}+A^{i-}\rightleftarrows H_4L^1A^{(4-i)}$. The constants corresponding to the latter equilibrium display the largest values for all the studied anionic substrates, which can be attributed to the maximization of interactions (electrostatic and H-bonding interactions) between the fully protonated receptor and fully deprotonated anion. On the other hand, the $H_5L^1A^{2+/3+}$ and $H_6L^1A^{3+}$ species are formed by reaction of the fully protonated macrocycle and partially protonated anions, while the species with lower number of protons are formed by the association of the partially protonated macrocycle and the fully deprotonated anions. Values of the stepwise constants are show in Table 2.

As expected the largest K_{eff} value was found for btc^{3-} followed by iph^{2-}, see Figure 2 and Table 2. However, the values for the different substrates are relatively low and only small differences were observed between them. In spite of this, it is interesting to note that the three structural aromatic isomers (ph^{2-}, iph^{2-}, and

Table 1
Overall association constants ($\log \beta_{H_hL^1A_a}$)[a] for the equilibria of $(H_iL^1)^{i+}$ with suc^{2-}, cta^{3-}, ph^{2-}, iph^{2-}, tph^{2-} and btc^{3-}

Equilibrium process	suc^{2-}	cta^{3-}	ph^{2-}	iph^{2-}	tph^{2-}	btc^{3-}
$6H^++L^1+A^{3-}\rightleftarrows H_6L^1A^{3+}$	—	44.41(5)	—	—	—	43.0(1)
$5H^++L^1+A^{i-}\rightleftarrows H_5L^1A^{(5-i)}$	—	40.37(3)	40.54(3)	40.57(3)	—	40.34(2)
$4H^++L^1+A^{i-}\rightleftarrows H_4L^1A^{(4-i)}$	35.26(2)	36.22(1)	35.99(2)	36.43(2)	35.63(3)	36.72(8)
$3H^++L^1+A^{i-}\rightleftarrows H_3L^1A^{(3-i)}$	27.54(9)	28.15(4)	28.60(2)	29.12(2)	28.20(5)	28.99(1)
$2H^++L^1+A^{i-}\rightleftarrows H_2L^1A^{(2-i)}$	—	—	20.59(2)	20.94(3)	20.19(6)	20.64(2)
$H^++L^1+A^{i-}\rightleftarrows HL^1A^{(1-i)}$	—	—	—	12.07(3)	—	—

I=0.10 M in KCl at 298.2 K.
[a] Values in parentheses are standard deviations on the last significant figure. A is the anion.

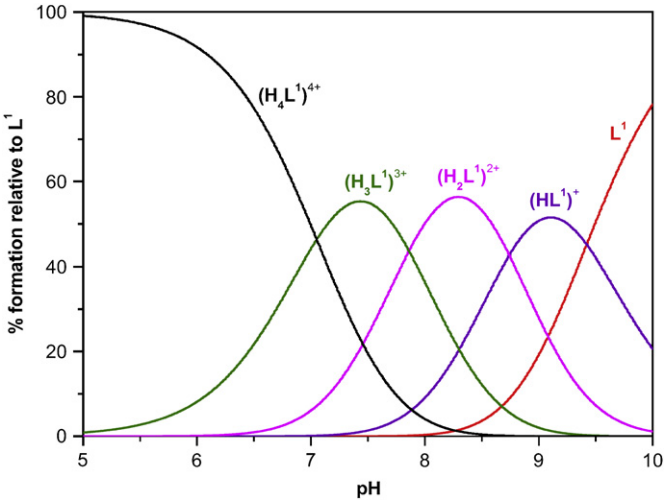

Figure 1. Distribution curve diagram of the studied receptor. $C_L^1=3.0\times10^{-3}$ M.

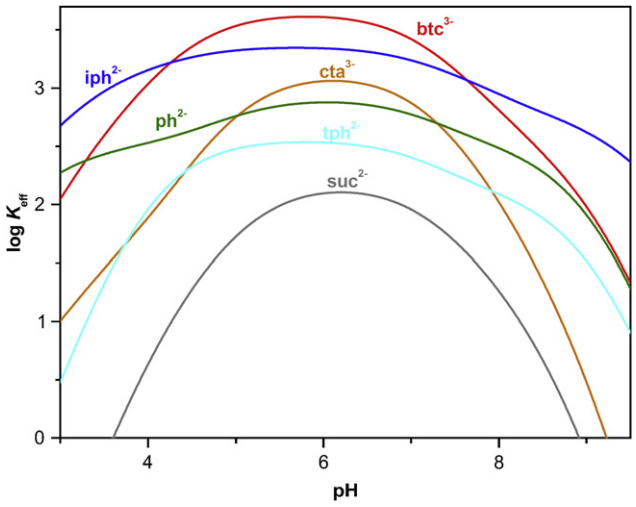

Figure 2. Plots of log K_{eff} versus pH for the associations between $(H_iL^1)^{i+}$ and the studied anionic substrates, $C_L^1=C_A=3.0\times10^{-3}$ M.

Table 2
Stepwise association constants ($\log K_{H_hL^1A_a}$) of $(H_{4-i}L^1)^{(4-i)+}$ and the different anionic substrates[a]

Equilibrium process	suc^{2-}	cta^{3-}	ph^{2-}	iph^{2-}	tph^{2-}	btc^{3-}
$(H_4L^1)^{4+}+H_2A^{-} \rightleftarrows H_6L^1A^{3+}$	—	1.78	—	—	—	1.90
$(H_4L^1)^{4+}+HA^{i-} \rightleftarrows H_5L^1A^{(4-i)}$	—	2.13	2.52	3.30	—	2.73
$(H_4L^1)^{4+}+A^{i-} \rightleftarrows H_4L^1A^{(4-i)}$	2.19	3.15	2.92	3.36	2.56	3.65
$(H_3L^1)^{3+}+A^{i-} \rightleftarrows H_3L^1A^{(3-i)}$	1.52	2.13	2.58	3.10	2.18	2.97
$(H_2L^1)^{2+}+A^{i-} \rightleftarrows H_2L^1A^{(2-i)}$	—	—	2.43	2.78	2.03	2.48
$(HL^1)^{+}+A^{i-} \rightleftarrows HL^1A^{(1-i)}$	—	—	—	2.65	—	—

I=0.10 M in KCl at 298.2 K.
[a] The deprotonated anion is represented by A.

tph^{2-}) have quite different association constants, following the order $iph^{2-}>ph^{2-}>tph^{2-}$. The three anions have similar basicity, the same charge, but their charge density follow the order $ph^{2-}>iph^{2-}>tph^{2-}$. Consequently, the trend of their association constants cannot be explained by any of these factors, otherwise structural factors may play a crucial role, see below.

In Figure 3 is shown the speciation diagrams corresponding to the species formed between $(H_iL^1)^{i+}$ and tph^{2-} (right) and btc^{3-} (left) anions, where the differences of binding strength with both anions can be visualized. In both cases, the main species is $H_4L^1A^{2+/+}$ and appears at a large pH range, however, the amount in solution of $[H_4L^1(btc)]^{+}$ is about double of $[H_4L^1(tph)]^{2+}$, and the amount of the $H_3L^1A^{+}$ and H_2L^1A (A=tph^{2-}) species formed at high pH is very low (<15%).

From all the anions studied, suc^{2-} exhibits the lowest association constant. This can be attributed to its high conformational freedom and low charge density.

3. ^{1}H NMR spectroscopy

^{1}H NMR spectroscopic titrations were performed in D_2O at pD about 6 (see Fig. S1 of Supplementary data, the ^{1}H NMR titration curves of the macrocycle as a function of pD). The ionic strength was not controlled to avoid interfering anions and Cl^{-} was chosen as the receptor counterion. These experimental conditions led to the best resolution of spectra.

The ^{1}H NMR spectrum of $(H_4L^1)^{4+}$ consists of two singlets, H_a and H_b protons, and two triplets, H_c and H_d protons of –NCH_2CH_2O– chains (see numbering in Scheme 1). The fast exchange between the free and assembled molecules compared to the NMR time scale led to separated ^{1}H NMR signals for the receptor and the anion protons upon formation of the receptor–anion entity.

All the receptor $(H_4L^1)^{4+}$ protons are upfield shifted upon addition of the btc^{3-} solution, except H_d, which can be attributed to the repulsion of the neighboring oxygen atom by the close presence of the negative charge of the carboxylate group. Saturation is achieved upon addition of 1 equiv of anionic substrate. The observed H_a, H_b, and H_c shifts indicate that the ammonium groups and the aromatic spacers are involved in the association process by π–π stacking, H-bonding, and electrostatic interactions. The addition of the other studied anionic substrates to the receptor causes smaller shifts to all the protons when compared to btc^{3-} indicating weaker associations (Fig. 4). The ph^{2-} substrate exhibited the smallest H_a shift, which was of the same order of those observed with non-aromatic substrates such as cta^{3-}, suggesting that π–π stacking interaction is not responsible for the association process.

The ^{1}H NMR titration data were also used to determine the association constants, in spite of the lower accuracy of the determinations when compared to the potentiometric method and the different solvent used (D_2O instead of H_2O). In Table 3 are compiled the values determined using the HypNMR program[32] and in Figure 4 are shown the Δδ (δ=chemical shift) of two receptor protons as a function of the number of equivalents of the anionic substrate added.

The values calculated by the ^{1}H NMR titrations (Table 3) are of the same order of those determined by potentiometry. The differences can be attributed to the aforementioned different experimental conditions used in both techniques.

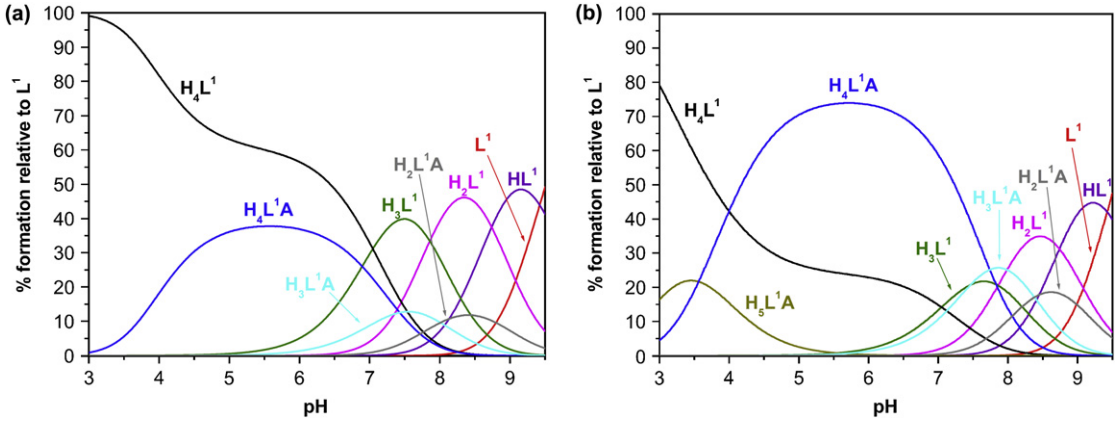

Figure 3. Distribution curves diagram of $(H_iL^1)^{i+}$ in the presence of the tph^{2-} anion (A) (left) and btc^{3-} anion (right). In both cases A=anion; $C_L^1=C_A=3\times10^{-3}$ M. The charges were omitted for clarity.

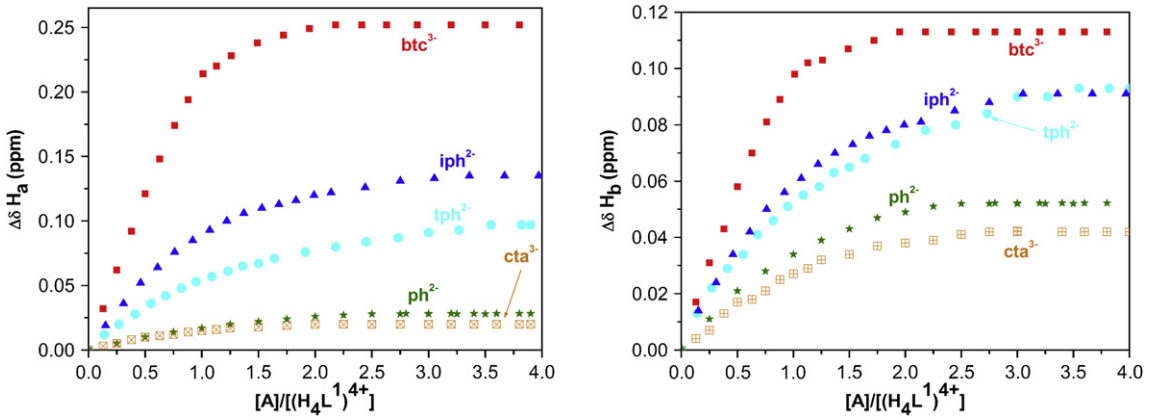

Figure 4. ^{1}H NMR titrations of $(H_4L^1)Cl_4$ with the studied anions, $\Delta\delta$ of the protons of the receptor as a function of the number of equivalents of substrate added, in D_2O, following the singlet H_a (left) and H_b (right) of the receptor.

Table 3
Association constants (log *K*) of $(H_4L^1)^{4+}$ with the studied anions[a]

Anion	log K[b]
btc^{3-}	3.94(2)
iph^{2-}	3.76(1)
ph^{2-}	3.29(1)
tph^{2-}	2.78(1)
cta^{3-}	3.46(1)

[a] Determined in D_2O at 300 K.
[b] Values in parentheses are standard deviations in the last significant figure given directly by the HypNMR program.[32]

3.1. X-ray crystal structures

The crystal structures of $(H_4L^1)^{4+}$ and its associated entities with ph^{2-} and tph^{2-} anions were determined by X-ray diffraction.

The asymmetric unit of the protonated receptor is composed of one-half of the macrocyclic cation, two PF_6^- counterions, and two water molecules. In addition, in the solid state, this compound exhibits *C*2 symmetry with a water molecule located on a twofold crystallographic symmetry axis perpendicular to the macrocyclic plane. This description is consistent with the molecular formula $(H_4L^1)(PF_6)_4\cdot 3H_2O$, **1**. The overall structure of **1**, excluding the PF_6^- anions, is shown in Figure 5 in two different views together with the atomic notation scheme adopted. The water molecule, O(300), on the twofold axis is located above the two phenyl rings, 1.361 Å away from the mass center of the receptor, while the remaining two water molecules are inside the macrocyclic cavity. The three water molecules are held together by two O–H···O hydrogen bonds with H···O distances of 1.89 Å. Subsequently, this water bridge establishes four O–H···N hydrogen bonding interactions with N···H distances of 1.94 and 1.95 Å. The crystal packing diagram of **1**, presented in Figure 6, shows that $(H_4L^1)^{4+}$ and PF_6^- anions are found in a 2-D network assembled via N–H···F hydrogen bonds. The dimensions of all hydrogen bonds found in the solid state for protonated receptor **1** are given in Table 4 together with those reported for **2** and **3**.

The asymmetric unit of **2** contains two independent half moieties of $(H_4L^1)^{4+}$, one entire molecule of ph^{2-}, and two PF_6^- anions, while the asymmetric unit of **3** is composed of one-half of $(H_4L^1)^{4+}$, one-half of tph^{2-}, and one PF_6^- anion, which is disordered over two octahedral positions. The content of the asymmetric units of these two compounds is completed with one water molecule leading to the general formula $[(H_4L^1)(A)](PF_6)_2\cdot H_2O$ (A=ph^{2-}, **2**; A=tph^{2-}, **3**). The overall structure of $(H_4L^1)^{4+}$ in the $[(H_4L^1)(A)]^{2-}$ supramolecular entity is presented in two different views in Figure 7 for ph^{2-} and in Figure 8 for tph^{2-}. In both figures (a) shows the centrosymmetric structure adopted by $(H_4L^1)^{4+}$ in these two compounds and the atomic notation, while in (b) is illustrated the macrocyclic conformation and the position of the anion relative to the receptor. Both anions are clearly outside the macrocyclic cavity giving rise to distances between the mass center of the anion determined by the aromatic carbon atoms and the N_4 macrocyclic plane of 3.081 Å (in **2**) and 3.076 Å (in **3**) for ph^{2-} and tph^{2-}, respectively.

A further insight into the associations between $(H_4L^1)^{4+}$ and the ph^{2-} and tph^{2-} anions is given by the crystal packing diagrams presented in Figure 9. In both compounds, the anions assemble $(H_4L^1)^{4+}$ ions via multiple N–H···O hydrogen bonds in 1-D chains, which run along the base vectors [010] and [010] for the species with ph^{2-} and tph^{2-}, respectively. The supramolecular interaction between $(H_4L^1)^{4+}$ and tph^{2-} involves six N–H binding sites and only three oxygen atoms from carboxylate groups with the formation of three independent N–H···O hydrogen bonds with H···O distances of 1.95, 1.85, and 2.10 Å. The remaining two N–H binding groups establish with solvent water molecules N–H···O=C hydrogen bonds with H···O distances of 2.21 Å. In addition, for compound

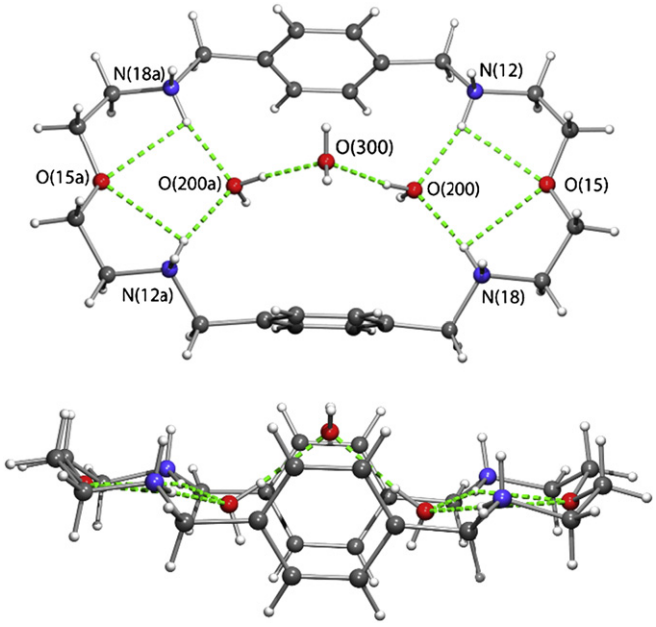

Figure 5. Molecular diagrams of $(H_4L^1)^{4+}$ showing the overall structure with labeling scheme adopted (top) and the relative position of water molecules to the macrocyclic cavity (bottom); *a* denotes the symmetry operation: 1−*x*, *y*,1/2−*z*.

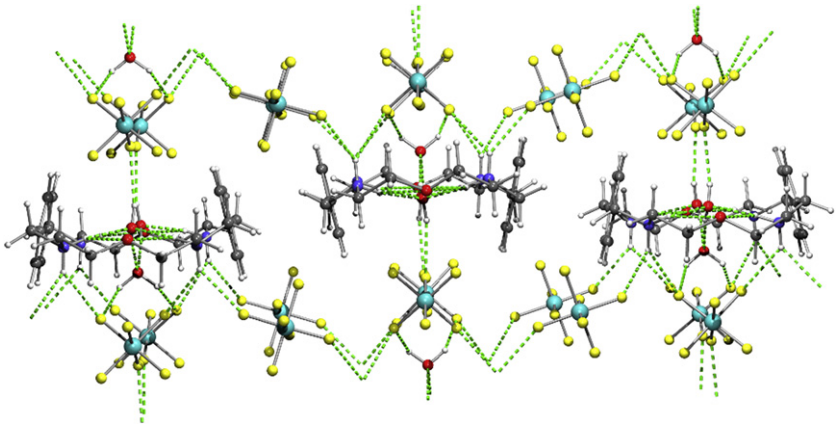

Figure 6. Crystal packing of $(H_4L^1)(PF_6)_4\cdot 3H_2O$, **1**, showing the 2-D network of N–H···F hydrogen bonds.

3 several short intermolecular contacts between N–H groups and the fluorine atoms are also found but they were excluded from the hydrogen bond analysis because of the disorder exhibited by the PF_6^- counterion. In compound **2**, the ph^{2-} anion bridges two independent molecules of $(H_4L^1)^{4+}$ through seven concomitant N–H···O hydrogen bonds between the four oxygen atoms of two carboxylate groups and seven N–H binding sites with H···O distances ranging from 1.76 to 2.35 Å (see Table 4). The eighth N–H···O hydrogen bonding interaction involves the second independent $(H_4L^1)^{4+}$ macrocycle and the water solvent molecule with an H···O distance of 2.21 Å. One N–H···F hydrogen bonding interaction (H···F=2.10 Å) between an N–H binding group from the first independent $(H_4L^1)^{4+}$ and one PF_6^- anion completes the pattern of hydrogen bonds found in the solid state for this supramolecular entity.

The $(H_4L^1)^{4+}$ cation in the three compounds adopts conformations with the phenyl rings almost parallel as can been seen in Figures 5, 7a, and 8a. However, the endocyclic torsion angles listed in Table 5 show that these conformations are different. This result is expected taking into account the C_2 and C_i symmetries found for $(H_4L^1)^{4+}$. In addition, in the supramolecular entity with tph^{2-}, O–H···O hydrogen bonds occur between the water molecule and the oxygen atom from $(H_4L^1)^{4+}$ (H···O distance of 2.20 Å), which indicates that packing effects play an important role in the conformation adopted by $(H_4L^1)^{4+}$ in the solid state.

Table 4
Dimensions of the hydrogen bonds in solid state of $(H_4L^1)^{4+}$ and of the association entities of $(H_4L^1)^{4+}$ with ph^{2-} and tph^{2-}

	H···A/Å[a]	D···A/Å[a]	D–H···A/°
$(H_4L^1)(PF_6)_4\cdot 3H_2O$ **1**			
N(12)–H(13a)···F(21) [x, $-y+1$, $z-1/2$]	2.21	2.930	137
N(12)–H(13a)···F(12) [$-x+1/2$, $y-1/2$, $-z+1/2$]	2.34	3.039	135
N(18)–H(18A)···F(23)	2.47	3.104	128
N(18)–H(18A)···F(13) [$-x+1/2$, $y-1/2$, $-z+1/2$]	2.47	3.175	136
N(12)–H(13b)···O(200)	1.95	2.822	163
N(18)–H(18B)···O(200)	1.94	2.826	166
O(200)–H(201)···O(300)	1.89	2.713	173
O(200)–H(202)···F(11) [$-x+1/2$, $y+1/2$, $-z+1/2$]	2.12	2.934	167
O(200)–H(202)···F(15) [$-x+1/2$, $y+1/2$, $-z+1/2$]	2.62	3.132	121
O(300)–H(301)···F(13) [$x+1/2$, $y-1/2$, z]	2.55	2.993	115
$[(H_4L^1)(ph)](PF_6)_2\cdot H_2O$ **2**			
N(12)–H(13a)···O(511)	1.83	2.728	173
N(12)–H(13b)···O(522)	2.08	2.872	146
N(18)–H(18A)···O (521)	2.35	2.935	122
N(18)–H(18B)···O (522)	1.94	2.749	150
N(32)–H(33b)···O (512) [x, $y+1$, z]	1.76	2.656	175
N(32)–H(33b)···O (511) [x, $y+1$, z]	2.62	3.240	127
N(38)–H(38A)···O (512) [$-x+3$, $-y$, $-z$]	2.19	2.893	134
N(38)–H(38B)···O (521) [$-x+3$, $-y$, $-z$]	1.80	2.688	167
N(18)–H(18A)···F(22) [$x+1$, y, z]	2.10	2.886	145
N(32)–H(33a)···O (100)	2.19	2.952	142
$[(H_4L^1)(tph)](PF_6)_2\cdot H_2O$ **3**			
O(100)–H(101)···O(15)	2.20	2.878	138
N(12)–H(13b)···O(341) [$x+1$, y, z]	1.95	2.773	151
N(18)–H(18A)···O (341) [$x+1$, y, z]	1.85	2.721	161
N(18)–H(18B)···O (342)	2.10	2.949	156
N(12)–H(13a)···O(100)	2.21	3.002	147

[a] A and D mean a proton acceptor and receptor, respectively.

3.2. Molecular modeling studies

The binding affinity of $(H_4L^1)^{4+}$ for the tph^{2-} and btc^{3-} anionic substrates was investigated with Amber 9[33] using the GAFF force field.[34] This theoretical study comprises conventional molecular dynamics (MD) simulations in water solution followed by binding free energy calculations using the MM–PBSA method (Molecular Mechanics/Poisson–Boltzmann Surface Area).[35] The binding association models were generated by docking the structures of $(H_4L^1)^{4+}$ and of anions, using low mode (LMOD) search, as described in Section 5. The systematic search of the conformational space yielded 100 lowest energy binding scenarios within the narrow energy range of 7.4 kcal mol^{-1} for tph^{2-} and of 3.4 kcal mol^{-1} for btc^{3-}. Two minimized molecular mechanics structures for both associated entities were selected by primarily taking into account the number of hydrogen bonds and the relative position of the anion to the receptor. For the tph^{2-} anion in the first binding arrangement (**3a**), the anion is located above the receptor, roughly parallel to the N_4 macrocyclic plane, with the two carboxylate groups forming five C═O···N–H hydrogen bonds with all four nitrogen proton donors. By contrast, in the second model (**3b**) the anion is almost encapsulated into the receptor cavity with the carboxylate groups forming also five C═O···N–H hydrogen bonds but with only three nitrogen centers. These structures are shown in Figure 10. For btc^{3-}, in binding arrangement **4a**, the anion is also positioned above the receptor but it adopts a spatial disposition tilted relatively to the N_4 receptor plane whereas in the binding arrangement **4b**, the anion is almost encapsulated in the macrocyclic cavity adopting a spatial disposition parallel to the two phenyl rings, which is consistent with π–π interactions. Furthermore, these two binding arrangements are stabilized by multiple C═O···N–H hydrogen bonding interactions between two carboxylate groups and three N–H binding sites, seven for **4a** and five for **4b** as shown in Figure 11.

Subsequently, the dynamic behavior of the two binding scenarios for each assembled molecule was evaluated through conventional MD simulations in water solution carried out for 15 and 10 ns for the tph^{2-} and btc^{3-} systems, respectively. The variation of the intermolecular distances between the mass centers of the

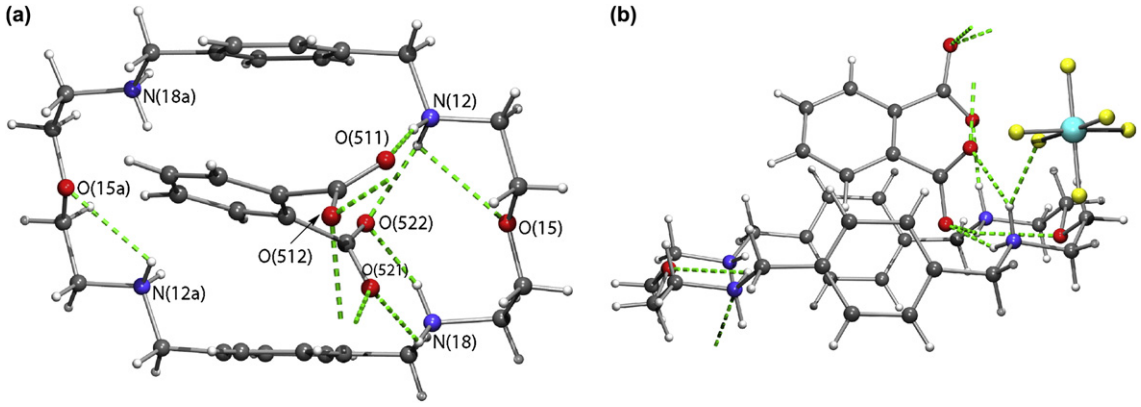

Figure 7. Two different perspectives showing the interaction of one centrosymmetric cation $(H_4L^1)^{4+}$ with one ph^{2-} anion: (a) shows the hydrogen bonds between cation and anion (the centrosymmetrically related ph^{2-} anion is omitted for clarity); (b) emphasizes the spatial dispositions of ph^{2-} and a PF_6^- counterion relatively to the receptor (right) as well as the macrocyclic conformation; *a* corresponds to the symmetry operation 3−*x*, −*y*, −*z*.

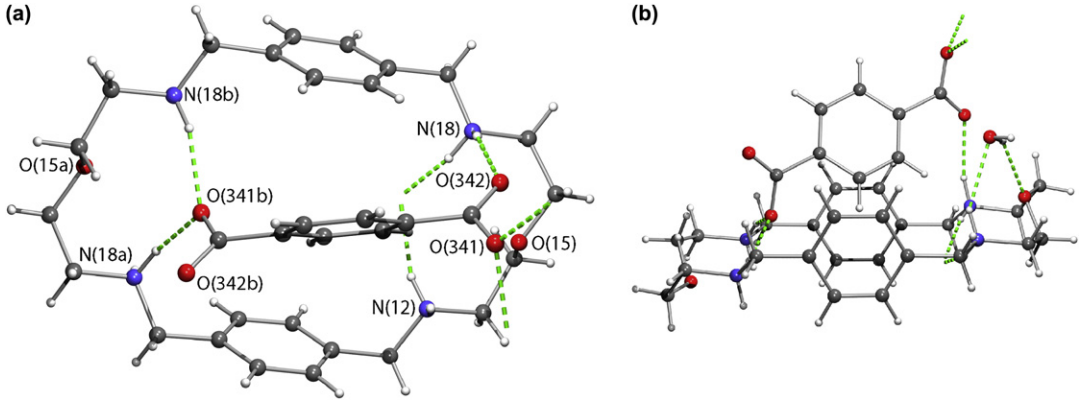

Figure 8. Two different views showing the interaction of one centrosymmetric cation $(H_4L^1)^{4+}$ with one tph^{2-} anion: (a) shows the hydrogen bonds between cation and anion (the centrosymmetrically related tph^{2-} anion is omitted for clarity); (b) emphasizes the spatial disposition of the tph^{2-} anion and solvent water molecule relative to the receptor and the macrocyclic conformation; *a* and *b* represent the symmetry operations 2−*x*, 1−*y*, 2−*z* and 1−*x*,1−*y*, 2−*z*, respectively.

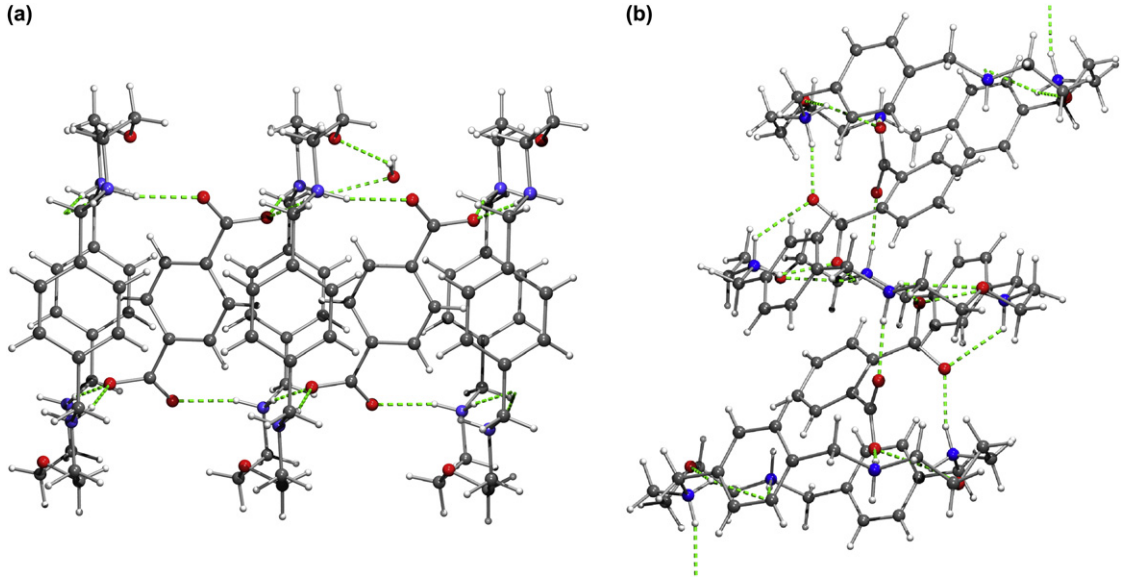

Figure 9. Crystal packing diagrams showing the assembling in 1-D chains of $(H_4L^1)^{4+}$ molecules with (a) tph^{2-} (**3**) and (b) ph^{2-} (**2**) via N–H···O hydrogen bonds.

receptor and the anionic substrates ($C_R \cdots C_A$), determined by the four nitrogen donor atoms from the receptor and the aromatic carbon atoms of the anions, is plotted in Figure 12 for tph^{2-} and btc^{3-} anions.

In the simulation carried out with the binding arrangement **3b** (red line), the tph^{2-} remains encapsulated during the first ca. 6 ns, then it moves to the top during the next 1 ns, after that it leaves the receptor until 11 ns of simulation. After that time, the anion enters

Table 5
Independent endocyclic torsion angles (°) for $(H_4L^1)^{4+}$ in the free receptor **1** and in the associated entities with ph^{2-} **2** and tph^{2-} **3**

Central bond	**1**	**2**[b]		**3**
C_{Ar}–C[a]	106.8(5)	−94.0(7)	*−90.6(8)*	−90.8(6)
C–N	−165.3(4)	172.4(5)	*165.1(5)*	−175.4(4)
N–C	−178.2(4)	−178.0(5)	*−172.5(5)*	165.6(4)
C–C	−62.6(5)	71.9(6)	*74.0(6)*	56.5(6)
C–O	173.3(4)	−179.3(5)	*170.0(6)*	171.2(4)
O–C	−178.4(3)	171.2(5)	*85.1(9)*	76.9(6)
C–C	61.7(5)	−70.5(7)	*54.2(10)*	53.9(6)
C–N	−173.7(4)	−179.4(6)	*−148.0(6)*	172.1(4)
N–C	−173.8(4)	−174.2(6)	*173.8(6)*	173.1(4)
C–C_{Ar}[a]	−113.7(5)	148.9(6)	*−105.3(7)*	−134.6(5)

[a] C_{Ar} means the aromatic carbon atoms directly bonded to the aliphatic linkage.
[b] The italic values correspond to the second molecule of $(H_4L^1)^{4+}$.

definitively into the macrocyclic cavity adopting a spatial disposition equivalent to that found in the first 5 ns of simulation. In the MD simulation with the binding arrangement **3a**, after the first 1 ns of simulation the binding interaction between the receptor and the tph^{2-} is interrupted until ca. 8 ns. Then, the binding interaction is restored, with the anion located above the macrocyclic receptor during 1 ns in a binding arrangement comparable to the starting geometry. After that the anion enters into the macrocyclic cavity, remaining encapsulated until the end of the simulation. These two simulations performed using different starting binding arrangements are equivalent over the simulation periods in which the tph^{2-} is encapsulated. Both simulations also indicate that the tph^{2-} has the propensity to leave the binding association with the receptor in water solution. The molecular recognition process between $(H_4L^1)^{4+}$ and tph^{2-} is illustrated in Figure 13 with several

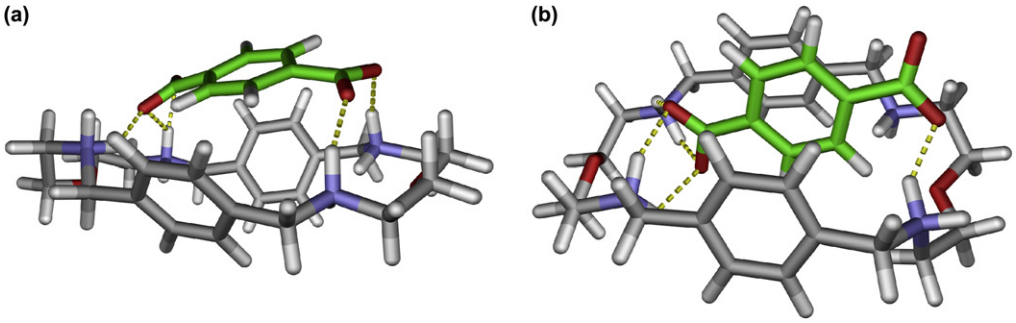

Figure 10. Binding interaction models between tph^{2-} and $(H_4L^1)^{4+}$ obtained via docking (a) model **3a**; (b) model **3b**.

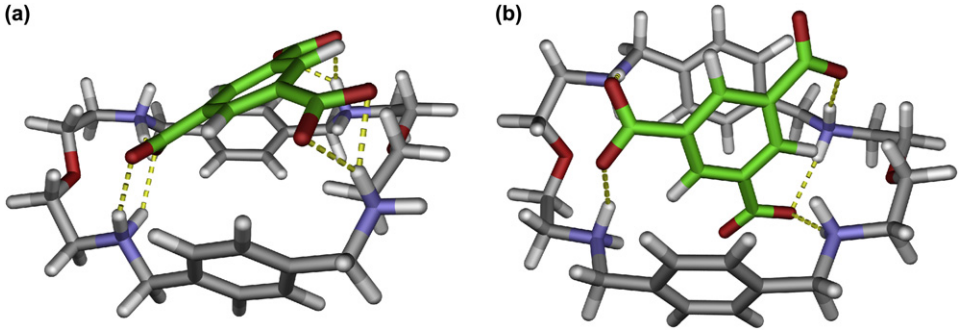

Figure 11. Binding interaction models of btc^{3-} with $(H_4L^1)^{4+}$ obtained via docking (a) model **4a**; (b) model **4b**.

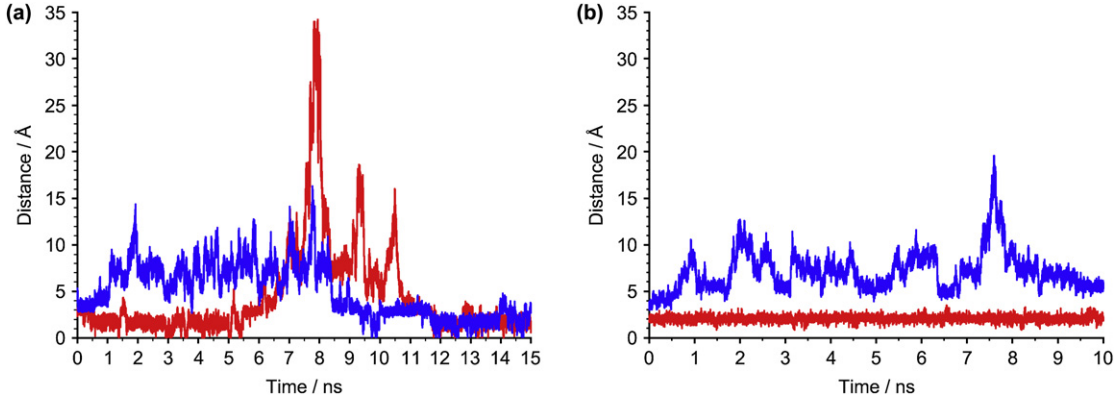

Figure 12. Evolution of the $C_R \cdots C_A$ distances for (a) tph^{2-} **3a** in blue and **3b** in red, and (b) btc^{3-} **4a** in blue and **4b** in red. MD simulations carried out with starting models with the anion located at the top of $(H_4L^1)^{4+}$ (blue line) and in the macrocyclic cavity (red line).

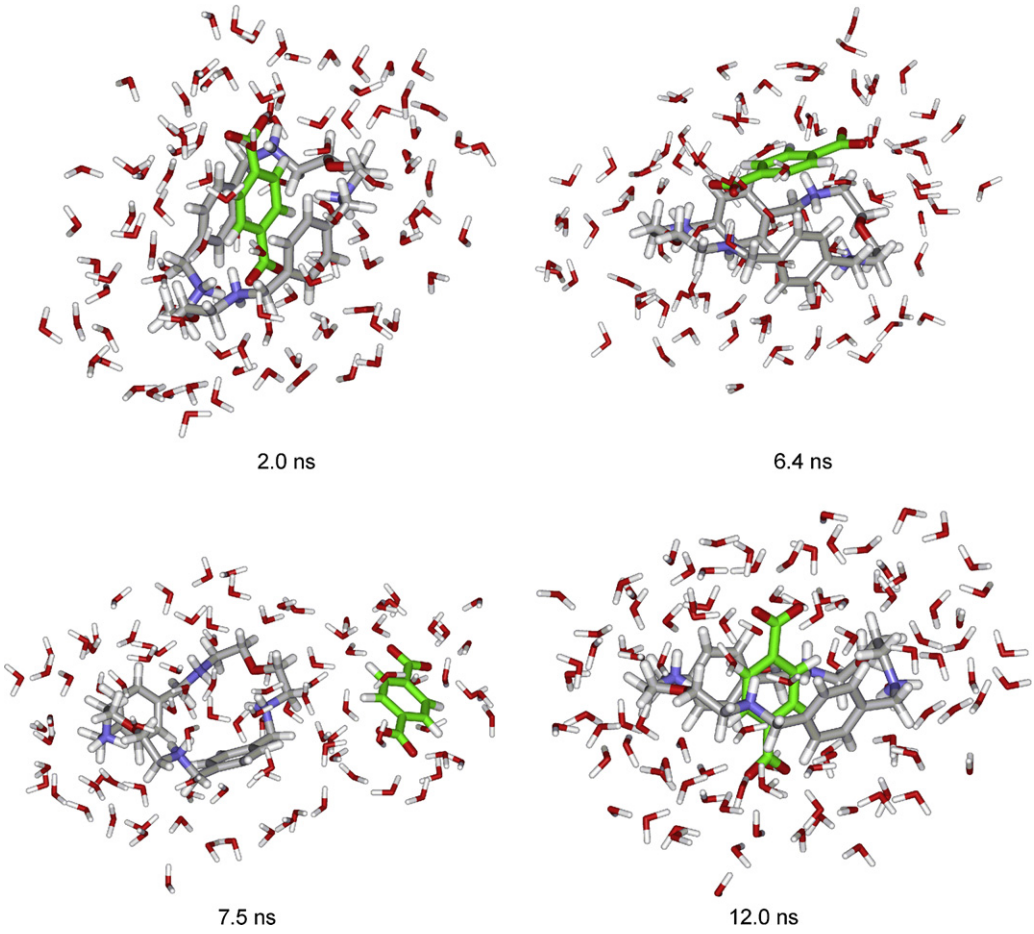

Figure 13. Snapshots taken from MD simulation carried out with model **3b** of $(H_4L^1)^{4+}$ with tph^{2-}. The closest solvent shell is composed of 100 water molecules. The chloride anions are omitted.

snapshots taken from the MD simulation performed with the starting model **3b**.

In the arrangement **4a**, the btc^{3-} anion remains at the top of the receptor up to 0.5 ns, and then it leaves the receptor breaking the binding association. Afterwards, the interactions are restored several times over short simulation periods after considerable longer periods where there is no significant short binding contacts between $(H_4L^1)^{4+}$ and btc^{3-}. By contrast in the arrangement **4b**, the btc^{3-} remains in the macrocyclic cavity for the entire time of the simulation forming a supramolecular entity with the substrate included.

The MD simulations show that the molecular recognition of both anions by the $(H_4L^1)^{4+}$ receptor is assisted by multiple and cooperative N–H···O=C hydrogen bonds. Those involving the interactions of tph^{2-} and btc^{3-} with the receptor were monitored. Thus the dimensions of the hydrogen bonds were calculated for tph^{2-} along the first 5 ns of the MD simulation carried out with the starting geometry **3b** and for btc^{3-} over the entire time of the MD simulation (10 ns) performed with the starting geometry **4b**, using a cut-off of 2.5 Å for H···O distances and 120° for the N–H···O=C angles. The hydrogen bonding interactions of $(H_4L^1)^{4+}$ and tph^{2-} occur mainly by means of two N–H···O=C short intermolecular contacts between one oxygen atom of the anion and two N–H binding sites adjacent to the *p*-phenyl spacers. The average H···O distances are 2.35 and 2.30 Å and the corresponding average N–H···O=C angles are 143 and 148°. The encapsulation of the btc^{3-} anion involves mainly four N–H···O=C hydrogen bonds between oxygen atoms from different carboxylate groups and four N–H binding sites from the four nitrogen acceptors. Two of the hydrogen bonds with average H···O distances of 2.13 and 2.12 Å and average N–H···O=C angles of 163 and 164° are quite strong whereas the remaining two with average H···O distances of 2.32 Å and average N–H···O=C angles of 146 and 145° are much weaker.

The binding free energies of $(H_4L^1)^{4+}$ toward the two aromatic anions were estimated theoretically through the post-processing of the single MD trajectories for the associations with btc^{3-} (model **4b**) and tph^{2-} (models **3a** and **3b**) with the MM–PBSA method.[35] The energetic and entropic contributions to the binding free energy of both anions are collected in Table 6. These average values for btc^{3-} were calculated with snapshots taken from the 10 ns of simulation while for tph^{2-} they were calculated for the first 5 ns of MD simulation with model **3b**. The analysis of the free energy components shows that the electrostatic term is the largest contributor for the molecular mechanics internal energy. Indeed, the Coulombic interactions stabilize the binding association by -233.6 kcal mol^{-1} for btc^{3-} and -150.5 kcal mol^{-1} for tph^{2-}, while the van der Waals interactions contribute only with ca. 14.0 kcal mol^{-1} for the stabilization of both associations. The electrostatic effect is partially counterbalanced by the unfavorable polar term of the solvation energy leading to an enthalpy (ΔG_{tot}) of -16.8 and -21.1 kcal mol^{-1} for the associations with tph^{2-} and btc^{3-}, respectively. A disfavored contribution of the entropy term $T\Delta S$ of -14.5 kcal mol^{-1} for tph^{2-} and -15.4 kcal mol^{-1} for btc^{3-} was obtained, leading to the relative binding free energies (ΔG_{bind}) of -2.4 kcal mol^{-1} for tph^{2-} and -5.7 kcal mol^{-1} for btc^{3-}. The value for tph^{2-} is underestimated by -1.3 and -2.5 kcal mol^{-1} relative to

Table 6
Binding free energy contributions (kcal mol^{-1}) for the interaction of $(H_4L^1)^{4+}$ with the aromatic anions tph^{2-} and btc^{3-}

Contribution[a]	tph^{2-}		btc^{3-}	
	Mean	σ[b]	Mean	σ
ΔE_{MM}	−164.46	0.06	−248.72	0.06
ΔG_{np}	−1.59	0.0	−1.78	0.0
ΔG_{PB}	149.23	0.05	229.42	0.05
ΔG_{solv}	147.64	0.05	227.64	0.05
ΔG_{tot}	−16.83	0.03	−21.08	0.03
$T\Delta S_{total}$	−14.48	0.02	−15.40	0.09
ΔG_{bind}	−2.35	0.04	−5.68	0.09

[a] ΔE_{MM}=molecular mechanics internal energy; $\Delta G_{solv}=\Delta G_{np}+\Delta G_{PB}$, being ΔG_{np}=nonpolar solvation free energy and ΔG_{PB}=polar solvation free energy; $\Delta G_{tot}=\Delta G_{solv}+\Delta E_{MM}$; $\Delta G_{bind}=\Delta G_{tot}-T\Delta S_{total}$.
[b] σ=Standard errors of mean values.

the values determined from potentiometric and ^{1}H NMR titrations, respectively. Identical theoretical values within 0.1 kcal mol^{-1} difference were determined from the last 6 and 4 ns of the MD simulations performed with the starting models **3a** and **3b**, respectively.

On the other hand, when the structures extracted from two entire simulations are included in calculations, positive unfavorable values for ΔG_{bind} are obtained. In other words, these theoretical findings suggest that the experimental binding data correspond to the encapsulation of tph^{2-} into the $(H_4L^1)^{4+}$ receptor. In line with this assessment, the estimated binding free energy for the btc^{3-} association is in excellent agreement with those calculated from potentiometric (−5.0 kcal mol^{-1}) and ^{1}H NMR data (−5.4 kcal mol^{-1}).

4. Conclusions

The molecular recognition ability of the receptor $(H_4L^1)^{4+}$ toward several carboxylate anions with different size, charge, and structure was evaluated. The binding studies were carried out by potentiometry and ^{1}H NMR spectroscopy in aqueous (or D_2O) solution. The first technique allowed the accurate determination of the association constants and the evaluation of all species formed at different pH values. The second one confirmed the binding ability of the receptor for the different anionic substrates. The quantitative values of the constants together with the magnitude of the shifts of each resonance of the receptor upon binding of the substrate allowed to envisage the type of interactions and location of the substrates in the assembled entity formed.

The X-ray structures of the supramolecular entities $[(H_4L^1)(A)](PF_6)_2\cdot H_2O$ (A=ph^{2-}, **2**; A=tph^{2-}, **3**) indicated that in the solid state both anionic substrates are located outside the receptor establishing multiple and cooperative N–H···O hydrogen bonding interactions. On the other hand, MD simulations in water solution confirmed the experimental solution results. They also showed that the binding constants correspond mainly to the encapsulation of tph^{2-} and btc^{3-} into the receptor with the enthalpic term of the binding free energy dictated by the balance of unfavorable polar solvation free energy and favorable molecular mechanics internal energy. The largest contributor for the later energy is the term corresponding to the electrostatic interactions, which incorporates all intermolecular interactions of this nature such as hydrogen bonds. However, the MD simulations also showed that the tph^{2-} anion leaves the receptor spontaneously, which is consistent with a weak interaction between the partners. These results are consistent with a molecular recognition process determined by a combination of electrostatic, hydrogen bonding, and π–π stacking interactions. The net charge of btc^{3-} has obviously an important role on the clear preference of the $(H_4L^1)^{4+}$ receptor for this carboxylate anion in water solution.

5. Experimental

5.1. General

Microanalyses were carried out by the ITQB Microanalytical Service. The ^{1}H and ^{13}C NMR spectra were recorded in a Bruker CXP 300 spectrometer.

Reagents. Terephthaldialdehyde and 1,5-diamino-3-oxapentane were obtained from Aldrich and Acros Organics, respectively. Succinic acid (99%) is a Merck product. 1,3,5-Benzene-tricarboxylic acid, terephthalalic acid (98%), phthalic acid (>99.5%), isophthalic acid (99%), and 1,3,5-cyclohexanetricarboxylic acid (95%) were purchased from Aldrich. All chemicals were of reagent grade and used as supplied. The references used for the ^{1}H NMR measurements in D_2O were 3-(trimethylsilyl)-propanoic acid-d_4–sodium salt. The macrocycle L^1 was synthesized according to the literature[36] and its tetraprotonated form $(H_4L^1)Cl_4$ was prepared by the addition of 0.1 M hydrochloric acid solution to L^1 in water solution (10 mL) till pH≈6. Then the solvent was evaporated to dryness and the solid recrystallized from ethanol and dried under vacuum before use. $(H_4L^1)Cl_4$: ^{1}H NMR (D_2O): δ (ppm) 3.87 (8H, t, NCH_2CH_2O), 3.43 (8H, t, NCH_2CH_2O), 4.26 (8H, s, $bzCH_2N$), and 7.45 (8H, s, bz). ESI-MS: *m*/*z* calcd: $[M+H]^+$=413.5, *m*/*z* exp: $[M+H]^+$=413.3.

5.2. Preparation of crystals for X-ray determination

*$(H_4L^1)(PF_6)_4$ (**1**)*. A solution of $(H_4L^1)(PF_6)_4$ (0.2 mmol, 0.112 g) was dissolved in ethanol/water (1:1 v/v, 5.0 mL) and left at rt. Crystals of quality suitable for X-ray analysis were obtained in 4 days. ^{1}H NMR (D_2O): δ (ppm) 3.87 (8H, t, NCH_2CH_2O), 3.43 (8H, t, NCH_2CH_2O), 4.26 (8H, s, $bzCH_2N$), and 7.45 (8H, s, bz).

*$[(H_4L^1)(ph)](PF_6)_2$ (**2**)*. To a solution of $(H_4L^1)(PF_6)_4$ (0.25 mmol, 0.140 g) in water (10 mL), at pH 6, 1 equiv of an aqueous solution of potassium phthalate (0.25 mmol, 0.06 g) at pH=6 was added. The solution was left stirring overnight and then evaporated, and the residue dissolved in ethanol/water (5.0 mL). Crystals of quality suitable for X-ray analysis were obtained in 3 days. ^{1}H NMR (D_2O): δ (ppm) 3.84 (8H, t, NCH_2CH_2O), 3.38 (8H, t, NCH_2CH_2O), 4.21 (8H, s, $bzCH_2N$), and 7.42 (8H, s, bz).

*$[(H_4L^1)(tph)](PF_6)_2$ (**3**)*. The procedure is similar to that used for **2** but using potassium terephthalate (0.25 mmol, 0.06 g). Crystals were also obtained in 3 days. ^{1}H NMR (D_2O): δ (ppm) 3.87 (8H, t, NCH_2CH_2O), 3.40 (8H, t, NCH_2CH_2O), 4.17 (8H, s, $bzCH_2N$), and 7.36 (8H, s, bz).

5.3. Potentiometric measurements

Reagents and solutions. Aromatic anions were prepared from the respective acids by the addition of 2 or 3 equiv of KOH in aqueous solution. The solutions were evaporated and the solid recrystallized from acetone. The anions were then standardized by titration using a standard HCl solution. The aliphatic anions were used in the acid form and standardized by titration with standard KOH. Carbonate-free solutions of KOH were freshly prepared, maintained in a closed bottle, and discarded when the percentage of carbonate was about 0.5% of the total amount of base (verified with the Gran method).[37,38] Demineralized water was used.

Equipment and working conditions. An Orion 720A measuring instrument was used together with a Metrohm glass electrode, an Orion 90-05 Ag/AgCl reference electrode, and a Wilhelm-type salt bridge containing 0.10 M KCl solution. A glass-jacketed titration cell (50 mL) completely sealed from the atmosphere was used and the temperature was controlled using a Grant W6 thermostat. Atmospheric CO_2 was excluded from the cell during the titration by passing purified N_2 across the top of the experimental solution. The standard base was added through a capillary tip at the surface of

the solution by a Metrohm Dosimat 665 burette. The temperature was kept at 298.2±0.1 K and the ionic strength of the solutions was maintained at 0.10±0.01 M in KCl.

Measurements. The $[H^+]$ of the solutions was determined by the measurement of the electromotive force of the cell, $E=E'^0+Q\log[H^+]+E_j$. The term pH is defined as $-\log[H^+]$. E'^0 and Q were determined by titrating a solution of known hydrogen-ion concentration at the same ionic strength, using the acid pH range of the titration. The value of $K_w=[H^+]\times[OH^-]$ was determined from the data obtained in the alkaline range of the titration, considering E'^0 and Q valid for the entire pH range, and found to be equal to $10^{-13.80}$ M^2. The liquid-junction potential, E_j, was found to be negligible under the experimental conditions used. The potentiometric equilibrium measurements were carried out using 20.00 mL of $\approx 2.05\times10^{-3}$ M of $(H_4L^1)^{4+}$ solutions diluted to a final volume of 30.00 mL, in the absence of dicarboxylate anions, and then in the presence of each anion at 1:1 and 1:2 C_L^l:C_A ratios. The E data were taken upon additions of 0.050 mL increments of the standard 0.10 M KOH solution.

Calculation of equilibrium constants. Overall protonation constants, β_i^H, were calculated by fitting the potentiometric data obtained for all the performed titrations with the HYPERQUAD program.[29] Protonation constants of the studied anions were also determined from the experimental data under the same experimental conditions also using the HYPERQUAD program. All these constants were taken as fixed values to obtain the binding constants of the new species from the experimental data corresponding to all the titrations at different C_L^l:C_A ratios. The initial computations were obtained in the form of overall stability constants, $\beta_{H_hL^lA_a}$ values, $\beta_{H_hL^lA_a}=[H_hL^lA_a]/[H]_h[L]^l[A]_a$. The errors quoted are the standard deviations of the overall stability constants given directly by the program for the input data, which include all the experimental points of all titration curves. The species considered in a particular model were those that could be justified by the principles of supramolecular chemistry. The binding constants of $(H_iL^1)^{i+}$ with the different anions were determined from a minimum of 100 (for tph^{2-}) to 151 (for cta^{3-}) experimental points and a minimum of two titration curves.

5.4. ^{1}H NMR titrations

Solutions of $(H_4L^1)Cl_4\approx 1.0\times10^{-3}$ M were prepared at pD≈6 in D_2O. The substrate solutions ($1.80–3.00\times10^{-2}$ M) were prepared from the potassium salt at pD≈6 in D_2O. To the solution of $(H_4L^1)Cl_4$ (0.5 mL), aliquots of anion salt solutions were added using a micropipette of 25 or 100 μL directly into the NMR tube. About 20 additions were necessary for each titration until no further change in the chemical shift was observed. Each solution was left 20–30 min to stabilize before measurements. All measurements were done at 300 K. No effort was made to maintain constant the ionic strength in order to avoid competition of other anions.

The association constants of the various species formed in solution were determined from the experimental titration data using HypNMR,[32] which requires as input the concentration of each component and the observed chemical shift. The fitting included the binding constants and the chemical shift of each species. Initial calculations provided overall stability constants, $\beta(H_nL^1)_nA_a$ values, $\beta(H_nL^1)_nA_a=[(H_nL^1)A_a]/[H_nL^1]_n[A]^a$. The errors quoted are the standard deviations of the overall stability constants given directly by the program from the input data, including the experimental points for all resonances of the titration curves.

5.5. Crystallography

The pertinent crystallographic data for compounds **1**–**3** are given in Table 7. X-ray data for compounds **1** and **3** were collected with an MAR research Image plate system with the crystals positioned at 70 mm from the image plate; 95 frames were taken at 2° intervals using an appropriate counting time. Data analysis was performed with the XDS program.[39] X-ray data for **2** were collected at 150 K on an X-Calibur CCD system from Oxford Diffraction Ltd. The crystal was positioned at 50 mm from the CCD and 321 frames were measured each for 10 s. Data analysis was carried out with software from the Crysalis software from Oxford Diffraction Ltd. All these collections were carried out with Mo Kα radiation (λ=0.71073 Å) and the crystallographic data are summarized in Table 7 with the pertinent refinement details.

Structures were solved by direct methods and by subsequent difference Fourier syntheses and refined by full matrix least squares on F^2 using the SHELX-97 suite.[40] Anisotropic thermal parameters were used for all non-hydrogen. Hydrogen atoms bonded to carbon and to nitrogen atoms were placed at calculated positions. The PF_6^- counterion was found to be disordered over two octahedral positions with four fluorine atoms occupying two alternative positions, which were included in refinement with refined occupancies of x and $1-x$. The atomic positions of hydrogen atoms of the water molecules of compounds **1** and **3** were taken from the last difference Fourier maps and they were refined with O–H and H···H

Table 7
Crystallographic data and selected refinement details for compounds **1**–**3**

	1	**2**	**3**
Molecular formula	$H_4L^1(PF_6)_4\cdot3(H_2O)$	$[H_4L^1(ph)](PF_6)_2\cdot(H_2O)$	$[H_4L^1(tph)](PF_6)_2\cdot(H_2O)$
Empirical formula	$C_{24}H_{46}F_{24}N_4O_5P_4$	$C_{32}H_{46}F_{12}N_4O_7P_2$	$C_{32}H_{48}F_{12}N_4O_8P_2$
M_w	1050.53	888.67	906.68
Crystal system	Monoclinic	Triclinic	Monoclinic
Space group	$C2/c$	$P-1$	$P2_1/c$
a/Å	26.015(28)	10.9310(10)	6.352(8)
b/Å	7.732(9)	13.2846(15)	20.570(23)
c/Å	20.699(25)	14.7490(9)	14.886(17)
α/°	(90)	84.884(12)	(90.0)
β/°	92.97(1)	68.091(7)	90.27(1)
γ/°	(90)	74.948(9)	(90.0)
V/Å^3	4158.0	1918.8(3)	1945.0
Z	4	2	2
D_c/Mg m^{-3}	1.678	1.538	1.548
μ/mm^{-1}	0.329	0.223	0.224
Reflections collected	9080	12,931	6378
Unique reflections [R_{int}]	3914 [0.0564]	12,931 [0.0295]	3128 [0.0742]
Final R indices			
R_1, wR_2 [$I>2\sigma I$]	0.0825, 0.1984	0.1164, 0.3949	0.0841, 0.1813
R_1, wR_2 (all data)	0.1037, 0.2109	0.1624, 0.3986	0.1135, 0.1685

distances restrained in order to reproduce ideal geometry. The hydrogen atoms bonded to water molecules of **2** were not apparent from the last difference Fourier maps and consequently their position was not inserted in the final structure refinement. All hydrogen atoms were refined with U_{iso}=1.2U_{eq} of the parent atom. The residual electronic density ranging from 0.61 to −0.49 e Å^{-3} for **1**, 0.76 to −0.51 e Å^{-3} for **2**, and 0.45 to −0.27 e Å^{-3} for **3** was within the expected values. Molecular diagrams were drawn with PLATON.[41]

5.6. Molecular modeling

All molecular modeling simulations and subsequent free energy calculations were carried out with the Amber 9 suite of programs,[33] using anions and receptor atomic parameters taken from the Gaff force field.[34]

The starting geometry of $(H_4L^1)^{4+}$ was generated from the crystal structure, while the structures of tph^{2-} and btc^{3-} were built using the Cerius 2 software package.[42] Partial atomic charges for the receptor and for the anions were calculated at the HF/6-31G* level by means of RESP methodology using the Gaussian 03 program.[43]

Docking between the receptor and both anions was investigated using the low mode (LMOD) search as implemented in Amber 9.[44] The anion was positioned above the receptor and the model binding association was energy minimized by molecular mechanics. The minimized structure was then used in a systematic search of conformational space using an implicit water model using a Metropolis criterion with *RT* equal to 1.5. The anions performed LMOD ZIG-ZAG moves between 0.1 and 10 Å from the $(H_4L^1)^{4+}$ cation. A total of 100 lowest energy binding arrangements were saved for the associations with tph^{2-} and btc^{3-}.

As mentioned above, two different starting geometries were selected to study the binding interaction between $(H_4L^1)^{4+}$ and the two anionic substrates, models **3a** and **3b** for tph^{2-} and models **4a** and **4b** for btc^{3-}. Subsequently, each one of these supramolecular associations was solvated with TIP3P water model[45] giving cubic boxes containing between 2046 and 2057 solvent molecules. Charge neutrality was achieved by placing one and two chloride anions outside the receptor for the systems boxes with btc^{3-} and tph^{2-}, respectively. These four systems were equilibrated under periodic boundary conditions using the following multistage protocol. The equilibration process started with the minimization of water molecules and Cl$^-$ counterions by molecular mechanics with 1000 steps by the steepest descent method followed by 10,000 steps of conjugate gradients keeping the structure of the supramolecular association receptor–anion rigid (solute) with positional restraints of 500 kcal mol^{-1} Å^{-2}. After minimization, the solvated system was heated up to 300 K over 50 ps using an NVT ensemble. Then, the positional restraint was removed and solvent density was adjusted at an average pressure of 1 atm through an MD simulation run of sufficient length (typically 250 ps) to adjust the density of the cubic box to the expected value for the liquid water at rt. Furthermore, at this stage the average value of the density remained constant at least during the last 100 ps of NPT simulation. Finally, data collection runs in an NPT ensemble at 300 K and 1 atm were carried out with equilibrated structures over 15 ns for tph^{2-} and 10 ns for btc^{3-} systems. The time step was 2 fs. Snapshots were saved every 0.2 ps. Bond lengths involving all bonds to hydrogen atoms were constrained with the SHAKE algorithm.[46] Particle Mesh Ewald method[47] was used to treat long-range electrostatic interactions and the non-bonded van der Waals interactions were truncated with a 12 Å cut-off. The binding free energy terms, listed in Table 6, for the binding associations between $(H_4L^1)^{4+}$ and tph^{2-} and btc^{3-} anions, were calculated by post-processing the trajectories of the MD simulations carried out with models **3b** and **4b** with the MM–PBSA method.[35] Snapshots of the individual species with solvent removed were taken from the MD trajectory file at intervals of 2 ps and a total of 2500 frames of the supramolecular entity $(H_4L^1)^{4+}$ with the anion were obtained using the first 5 ns of the MD simulation with tph^{2-}. For btc^{3-}, the 10 ns of MD simulation afforded 5000 frames of the three individual species. The solvation free energies and entropies were determined for each snapshot followed by averaging the energy values. The solvation free energies were calculated using a continuum representation of the solvent. The first term (G_{PB}) was estimated by solving the Poisson–Boltzmann equation for zero salt concentration with Delphi[48] and using a solute interior dielectric constant of 3.0. The value of G_{np} was determined from the solvent accessible area. The entropic contribution was estimated via the normal mode analysis as implemented in Amber 9.

Acknowledgements

The authors acknowledge the financial support from Fundação para a Ciência e a Tecnologia (FCT) and POCI, with co-participation of the European Community fund FEDER (Project no. POCI/QUI/56569/2004). S.C. also acknowledges FCT for the grant (SFRH/BD/13793/2003). We thank EPSRC and the University of Reading for funds for the MAR Image Plate and Oxford Diffraction X-Calibur systems.

Supplemetary data

Protonation constants of $(H_4L^1)^{4+}$ in aqueous solution (Table S1) and ^{1}H NMR titration curves of the macrocycle as a function of pD (Fig. S1). Supplementary data associated with this article can be found in the online version, at doi:10.1016/j.tet.2008.03.002.

References and notes

1. Oshovsky, G. V.; Reinhoudt, D. N.; Willem, V. *Angew. Chem., Int. Ed.* **2007**, *46*, 2366.
2. Gale, P. A. *Coord. Chem. Rev.* **2003**, *240*, 191.
3. Steed, J. W.; Atwood, J. L. *Supramolecular Chemistry*; John Wiley: Chichester, UK, 2002.
4. Lehn, J.-M. *Supramolecular Chemistry*; VCH: Chichester, UK, 1995.
5. Bianchi, A.; Bowman-James, K.; García-España, E. *Supramolecular Chemistry of Anions*; John Wiley: Chichester, UK, 1997.
6. Steed, J. W.; Turner, D. R.; Wallace, K. *Core Concepts in Supramolecular Chemistry and Nanochemistry*; John Wiley: Chichester, UK, 2007.
7. Gale, P. A.; García-Garrido, S. E.; Garria, J. *Chem. Soc. Rev.* **2008**, *37*, 151.
8. Ilioudis, C. A.; Steed, J. W. *J. Supramol. Chem.* **2001**, *1*, 165.
9. Linton, B. R.; Goodman, M. S.; Fan, E.; van Arman, S. A.; Hamilton, A. D. *J. Org. Chem.* **2001**, *66*, 7313.
10. Katayev, E. A.; Boev, N. V.; Khrustalev, V. N.; Ustynyuk, Y. A.; Tananaev, I. G.; Sessler, J. L. *J. Org. Chem.* **2007**, *72*, 2886.
11. Baldini, L.; Casnati, A.; Sansone, F.; Ungaro, R. *Chem. Soc. Rev.* **2007**, *34*, 254.
12. Blondeau, P.; Segura, M.; Pérez-Fernández, R.; Mendoza, J. *Chem. Soc. Rev.* **2007**, *36*, 198.
13. Kang, S. O.; Hossain, M. A.; Bowman-James, K. *Coord. Chem. Rev.* **2006**, *250*, 3038.
14. Hosseini, M. W.; Lehn, J. M. *J. Am. Chem. Soc.* **1982**, *104*, 3525.
15. Dietrich, B.; Hosseini, M. W.; Lehn, J. M.; Sessions, R. B. *J. Am. Chem. Soc.* **1981**, *103*, 1282.
16. Bencini, A.; Bianchi, A.; Burguete, M. I.; García-España, E.; Luis, S. V.; Ramirez, J. A. *J. Am. Chem. Soc.* **1992**, *114*, 1919.
17. Dhaenens, M.; Lehn, J. M.; Vigneron, J.-P. *J. Chem. Soc., Perkin Trans. 2* **1993**, 1379.
18. Bencini, A.; Bianchi, A.; Burguete, M. I.; Dapporto, P.; Doménech, A.; Garcia-España, E.; Luis, S. V.; Paoli, P.; Ramirez, J. A. *J. Chem. Soc., Perkin Trans. 2* **1994**, 569.
19. Paris, T.; Vigneron, J. P.; Lehn, J. M.; Cesario, M.; Guilhem, J.; Pascard, C. *J. Inclusion Phenom. Macrocycl. Chem.* **1999**, *33*, 191.
20. Fitzmaurice, R. J.; Kyne, G. M.; Douheret, D.; Kilburn, J. D. *J. Chem. Soc., Perkin Trans. 1* **2002**, 841.
21. Nelson, J.; Nieywenhuyzen, M.; Pál, I.; Town, R. M. *Dalton Trans.* **2004**, 229.
22. Bazzicalupi, C.; Bencini, A.; Bianchi, A.; Borsari, L.; Giorgi, C.; Valtancoli, B. *J. Org. Chem.* **2005**, *70*, 4257.
23. Hodacová, J.; Chadim, M.; Závada, J.; Aguilar, J.; Garcia-España, E.; Luis, S. V.; Miravet, J. F. *J. Org. Chem.* **2005**, *70*, 2042.
24. Carvalho, S.; Delgado, R.; Fonseca, N.; Félix, V. *New J. Chem.* **2006**, *30*, 247.

25. García-España, E.; Díaz, P.; Llinares, J. M.; Bianchi, A. *Coord. Chem. Rev.* **2006**, *250*, 2952.
26. Filby, M. H.; Humphries, T. D.; Turner, D. R.; Kataky, R.; Kruusma, J.; Steed, J. W. *Chem. Commun.* **2006**, 156.
27. Ghosh, K.; Masanta, G. *Tetrahedron Lett.* **2006**, *47*, 2365.
28. Cruz, C.; Delgado, R.; Drew, M. G. B.; Félix, V. *J. Org. Chem.* **2007**, *72*, 4023.
29. Gans, P.; Sabatini, A.; Vacca, A. *Talanta* **1996**, *43*, 1739.
30. Carvalho, S.; Delgado, R.; Drew, M. G. B.; Félix, V.; Figueira, M.; Henriques, R. T. *Polyhedron* **2008**, *27*, 679.
31. Albelda, M. T.; Bernardo, M. A.; García-España, E.; Godino-Salido, M. L.; Santiago, V. L.; Melo, M. J.; Pina, F.; Soriano, C. *J. Chem. Soc., Perkin Trans. 2* **1999**, 2545.
32. Frassineti, C.; Ghelli, S.; Gans, P.; Sabatini, A.; Moruzzi, M. S.; Vacca, A. *Anal. Biochem.* **1995**, *231*, 374.
33. Case, D. A.; Darden, T. A.; Cheatham, T. E. I.; Simmerling, C. L.; Wang, J.; Duke, R. E.; Luo, R.; Merz, K. M.; Pearlman, D. A.; Crowley, M.; Walker, R. C.; Zhang, W.; Wang, B.; Hayik, S.; Roitberg, A.; Seabra, G.; Wong, K. F.; Paesani, F.; Wu, X.; Brozell, S.; Tsui, V.; Gohlke, H.; Yang, L.; Tan, C.; Mongan, J.; Hornak, V.; Cui, G.; Beroza, P.; Mathews, D. H.; Schafmeister, C.; Ross, W. S.; Kollman, P. A. *Amber 9*; University of California: San Francisco, CA, 2006.
34. Wang, J.; Wolf, R. M.; Caldwell, J. W.; Kollmann, P. A.; Case, D. A. *J. Comput. Chem.* **2004**, *25*, 1157.
35. Kollman, P. A.; Massova, I.; Kuhn, B.; Huo, S.; Chong, L.; Lee, M.; Lee, T.; Duan, Y.; Wang, W.; Donni, O.; Cieplak, P.; Srinivasan, J.; Case, D. A.; Cheatham, T. E., III. *Acc. Chem. Res.* **2000**, *33*, 889.
36. Carvalho, S.; Delgado, R.; Drew, M. G. B.; Félix, V. *Dalton Trans.* **2007**, 2431.
37. Gran, G. *Analyst (London)* **1952**, *77*, 661.
38. Rossotti, F. J.; Rossotti, H. J. *J. Chem. Educ.* **1965**, *42*, 375.
39. Kabsch, W. *J. Appl. Crystallogr.* **1988**, *21*, 916.
40. Sheldrick, G. M. *SHELX-97*; University of Göttingen: Göttingen, 1997.
41. Spek, L. *Platon, A Multipurpose Crystallographic Tool*; Utrecht University: Utrecht, The Netherlands, 1999.
42. *Cerius 2 version 4.2*; Molecular Simulations: San Diego, CA, 2000.
43. Frisch, M. J.; Trucks, G. W.; Schlegel, H. B.; Scuseria, G. E.; Robb, M. A.; Cheeseman, J. R.; Montgomery, J. A.; Vreven, T., Jr.; Kudin, K. N.; Burant, J. C.; Millam, J. M.; Iyengar, S. S.; Tomasi, J.; Barone, V.; Mennucci, B.; Cossi, M.; Scalmani, G.; Rega, N.; Petersson, G. A.; Nakatsuji, H.; Hada, M.; Ehara, M.; Toyota, K.; Fukuda, R.; Hasegawa, J.; Ishida, M.; Nakajima, T.; Honda, Y.; Kitao, O.; Nakai, H.; Klene, M.; Li, X.; Knox, J. E.; Hratchian, H. P.; Cross, J. B.; Bakken, V.; Adamo, C.; Jaramillo, J.; Gomperts, R.; Stratmann, R. E.; Yazyev, O.; Austin, A. J.; Cammi, R.; Pomelli, C.; Ochterski, J. W.; Ayala, P. Y.; Morokuma, K.; Voth, G. A.; Salvador, P.; Dannenberg, J. J.; Zakrzewski, V. G.; Dapprich, S.; Daniels, A. D.; Strain, M. C.; Farkas, O.; Malick, D. K.; Rabuck, A. D.; Raghavachari, K.; Foresman, J. B.; Ortiz, J. V.; Cui, Q.; Baboul, A. G.; Clifford, S.; Cioslowski, J.; Stefanov, B. B.; Liu, G.; Liashenko, A.; Piskorz, P.; Komaromi, I.; Martin, R. L.; Fox, D. J.; Keith, T.; Al-Laham, M. A.; Peng, C. Y.; Nanayakkara, A.; Challacombe, M.; Gill, P. M. W.; Johnson, B.; Chen, W.; Wong, M. W.; Gonzalez, C.; Pople, J. A. *Gaussian 03, Revision C.02*; Gaussian: Wallingford, CT, 2004.
44. Kolossváry, I.; Guida, W. C. *J. Am. Chem. Soc.* **1996**, *118*, 5011.
45. Jorgensen, W. L.; Chandrasekhar, J.; Madura, J. D.; Impey, R. W.; Klein, M. L. *J. Chem. Phys.* **1983**, *79*, 926.
46. Ryckaert, J. P.; Cicotti, G.; Berendsen, H. J. C. *J. Comput. Phys.* **1977**, *23*, 327.
47. Essmann, U.; Perera, L.; Berkowitz, M. L.; Darden, T.; Lee, H.; Perdensen, L. G. *J. Chem. Phys.* **1995**, *103*, 8577.
48. Rocchia, W.; Alexov, E.; Honig, B. *J. Phys. Chem. B* **2001**, *105*, 6507.